Published in final edited form as:
J Struct Biol. 2013 May ; 182(2): 164–172. doi:10.1016/j.jsb.2013.02.014.

THE RHODOPSIN-TRANSDUCIN COMPLEX HOUSES TWO DISTINCT RHODOPSIN MOLECULES

Beata Jastrzebska[1,*], **Philipe Ringler**[2], **Krzysztof Palczewski**[1,*], and **Andreas Engel**[1,2,*]

[1]Department of Pharmacology, School of Medicine, Case Western Reserve University, Cleveland, Ohio 44106-4965, USA [2]Center for Cellular Imaging and Nano Analytics (C-CINA), Biozentrum, University of Basel, Mattenstrasse 26, CH-4058 Basel, Switzerland

Abstract

Upon illumination the visual receptor rhodopsin (Rho) transitions to the activated form Rho*, which binds the heterotrimeric G protein, transducin (G_t) causing GDP to GTP exchange and G_t dissociation. Using succinylated concanavalin A (sConA) as a probe, we visualized native Rho dimers solubilized in 1 mM n-dodecyl-β-D-maltoside (DDM) and Rho monomers 5 mM in DDM. By nucleotide depletion and affinity chromatography together with crosslinking and size exclusion chromatography, we trapped and purified nucleotide-free Rho*•G_t and sConA-Rho*•G_t complexes kept in solution by either DDM or lauryl-maltose-neopentyl-glycol (LMNG). The 3-D envelope calculated from projections of negatively stained Rho*•G_t-LMNG complexes accommodated two Rho molecules, one G_t heterotrimer and a detergent belt. Visualization of triple sConA-Rho*•G_t complexes unequivocally demonstrated a pentameric assembly of the Rho*•G_t complex in which the photoactivated Rho* dimer serves as a platform for binding the G_t heterotrimer. Importantly, individual monomers of the Rho* dimer in the heteropentameric complex exhibited different capabilities to be regenerated with either 11-*cis* or 9-*cis*-retinal.

Keywords

G protein-coupled receptor; heterotrimeric G protein; photoactivated rhodopsin dimer; transmission electron microscopy; transducin

INTRODUCTION

G protein-coupled receptors (GPCRs) transduce signals across cellular membranes, and are involved in most physiological processes. Rhodopsin (Rho), the primary molecule in the visual signaling cascade of rod photoreceptor cells, is the most widely studied GPCR and a paradigm for understanding signal transduction. Upon absorption of a single photon Rho transitions to the activated state (Rho*), which catalyzes nucleotide exchange on multiple transducin (G_t) heterotrimers, providing an initial signal amplification (Hofmann et al., 2009; Palczewski, 2006; Sakmar et al., 2002). Down-stream events amplify the photon-

*Address correspondence to: Beata Jastrzebska, PhD, Krzysztof Palczewski, PhD, or Andreas Engel, PhD, Department of Pharmacology, School of Medicine, Case Western Reserve University, 10900 Euclid Ave, Cleveland, Ohio 44106-4965, USA; Phone: 216-368-4631; Fax: 216-368-1300; bxj27@case.edu, kxp65@case.edu or andreas.engel@case.edu.

induced signal to ultimately produce a detectable electric pulse, the visual signal processed by vertebrate brains. The first crystal structure determined for a GPCR was that of Rho (Palczewski et al., 2000), and Rho crystals have yielded the highest resolution native structure of any GPCR determined to date (Okada et al., 2004). The structure of Rho* has been solved (Salom et al., 2006), the interaction site between Rho and the G_t C-terminus structurally defined (Choe et al., 2011; Scheerer et al., 2008; Standfuss et al., 2011), and $G_{t\alpha}$ activation by Rho* characterized by site-directed spin labeling and spectroscopy (Van Eps et al., 2011) as well as by hydroxyl radical labeling and deuterium uptake in combination with mass spectrometry (Orban et al., 2012). But an unresolved question concerns the molecular function(s) of Rho dimers and higher oligomers observed in native disc membranes (Fotiadis et al., 2003).

Binding of a single heterotrimeric G protein to GPCR dimers and formation of pentameric complexes has been observed in reconstitution experiments involving the leukotriene B4 receptor BLT1 (Baneres et al., 2003), dopamine D2 receptor (Han et al., 2009), serotonin 5-HT4 receptor (Pellissier et al., 2011), photoactivated Rho (Jastrzebska et al., 2011b), and the metabotropic glutamate receptor (El Moustaine et al., 2012), each with its respective G protein. Extensive evidence indicates the existence of Rho dimers in native disc membranes (Fotiadis et al., 2003; Jastrzebska et al., 2006; Jastrzebska et al., 2004; Suda et al., 2004), and of other GPCRs dimers in living cells (serotonin receptor 5-HT2C (Herrick-Davis et al., 2006; Herrick-Davis et al., 2012), β_1-adrenergic receptor (Kobayashi et al., 2009), β_2-adrenergic receptor (b2AR) (Angers et al., 2001; Angers et al., 2000)). In contrast, the most detailed structural insight into the receptor-G protein interaction provided by the recently solved crystal structure of T4 lysozyme (T4L)-b2AR•Gs•nanobody complex indicates a binding stoichiometry of one receptor and one G protein (Rasmussen et al., 2011). This is supported by a two-dimensional projection analysis of negatively stained T4L-b2AR•Gs•nanobody complexes purified in lauryl-maltose-neopentyl-glycol (LMNG). The significant size-mismatch between the projection map and the receptor monomer was explained by an unusually large size of the LMNG micelles (Westfield et al., 2011).

Single receptor activation triggering a physiological response *in vitro* has been observed for some GPCRs (Whorton et al., 2007; Whorton et al., 2008). However, the molecular envelope of negatively stained native Rho*•G_t complexes purified in n-dodecyl-β-D-maltoside (DDM) accommodated two Rho molecules and one G_t, in agreement with biochemical analyses and the mass of the 220±12 kDa complex determined by electron scattering (Jastrzebska et al., 2011b). To resolve uncertainties about the composition of this GPCR-G protein complex, we prepared Rho*•G_t in LMNG and DDM, and chose sConA as a labeling probe for the Rho molecules. Visualization of the negatively stained sConA-Rho complexes solubilized in either 1 or 5 mM DDM, as well as the triple sConA-Rho*•G_t complex unequivocally revealed that photoactivation promotes assembly of a pentameric complex in which a Rho* dimer provides a binding platform for the G_t heterotrimer. Furthermore we show that the two Rho monomers constituting the Rho* dimer in the activated complex have distinct functional properties, as demonstrated by their different capabilities to be regenerated with either 11-*cis* or 9-*cis*-retinal.

RESULTS

Formation and visualization of sConA-Rho complexes

Purified bovine Rho was incubated with sConA to visualize whether the native Rho dimer (Fotiadis et al., 2003) exists in solution. The sConA-Rho complexes formed were submitted to size exclusion chromatography in buffer containing either 1 mM DDM (Fig. 1A, solid line, top panel) or 5 mM DDM (Fig. 1A, broken line, top panel). Gel filtration elution profiles were similar under both conditions with the elution peaks of the sConA-Rho

complexes significantly shifted towards larger structures relative to the elution peak of either sConA (Fig. 1A, middle panel) or Rho in 1 mM DDM (Fig. 1A, bottom panel). However, the profile obtained in 1 mM DDM (Fig. 1A, solid line, top panel) revealed a distinctly larger shift than that in 5 mM DDM (Fig. 1A, broken line, top panel).

TEM analysis of sConA-Rho complexes kept in 5 mM DDM revealed heterogeneous particle populations. Most of the tri-lobed complexes featured a central elongated density with similar spherical domains attached to both ends (Fig. 1B), whereas a minority of particles had a central domain consisting of two elongated particles (not shown). Class averages showed some central domains with a bi-modal appearance (Fig. 1B, asterisks). Size and shape of negatively stained sConA dimers documented that the central domain of the sConA-Rho complexes represents the sConA moiety (Fig. 1C). Negatively stained Rho in 1 mM DDM revealed two elongated bimodal domains separated by a stained groove (Fig. 1D). These dimers exhibited a length of 65±4 Å (n=12) and a width of 56±4 Å (n=12). Apparently, they have the capacity to bind two sConA dimers, as revealed by structures composed of two parallel sConA dimers with domains accounting for Rho on each side (Fig. 1E). Rho domains exhibited a width of 63 ± 4 Å in 1 mM DDM, and 40 ± 2 Å in 5 mM DDM, compatible with the dimensions of Rho dimers shown in Fig. 1D and Rho monomers observed previously (Jastrzebska et al., 2006).

Formation and visualization of native Rho*•G_t complexes

The Rho*•G_t complex was formed and purified by using sConA affinity chromatography as described previously (Jastrzebska et al., 2011b). Solubilized in DDM and bound to the resin, Rho was activated by light and then saturated with G_t. The resulting Rho*•G_t-DDM complex was eluted from the column with α-methyl-D-mannopyranoside and immediately crosslinked with DSG, a short (spacer arm 7.7 Å) Lys residue -Lys residue homobifunctional crosslinker, to prevent complex dissociation. The crosslinked Rho*•G_t complex was separated from free Rho and G_t by size exclusion chromatography and fractions containing the Rho*•G_t complex were gel-filtered again to assure protein homogeneity and/or to exchange DDM for LMNG (Fig. 2A). The Rho*•G_t-LMNG complex migrated faster than the Rho*•G_t-DDM complex (supplementary Fig. S1A), and its calculated molecular mass was ~280 kDa, 60 kDa larger than the mass of the complex in DDM (Jastrzebska et al., 2011b), indicating that LMNG forms larger micelles than DDM. SDS-PAGE analysis of these complexes revealed a protein band that migrated at a molecular mass of ~160 kDa, supporting a 2:1 Rho:G_t stoichiometry (2 Rho - 78 kDa + G_t - 86 kDa = 164 kDa) (Fig. 2B, left panel (LMNG) and supplementary Fig. S1B, left panel (DDM)). Immunoblotting with antibodies against $G_{t\alpha}$, $G_{t\beta}$ and Rho confirmed this composition of the Rho*•G_t complexes (Fig. 2B, right panels (LMNG) and supplementary Fig. S1B, right panel (DDM)).

Negatively stained Rho*•G_t-LMNG complexes revealed ~130 Å long particles with a variable width (Fig. 2C, left and right panels). Similar particles were found when Rho*•G_t was purified in DDM (supplementary Fig. S2), confirming our previous results (Jastrzebska et al., 2011b). Image pairs from the same area of untilted and tilted (45°) grids were used to select particles based on their dimensions in the untilted sample, yielding class averages that showed a tri-lobed complex (Fig. 2C, bottom panel). The 3D map calculated by refining the initial model against 12950 projections of Rho*•G_t-LMNG complexes accommodated the model constructed previously based on the 3D envelope of Rho*•G_t-DDM, taking into account all structural and chemical information available ((Jastrzebska et al., 2011b); Fig. 2D).

Visualization of purified sConA-Rho*•G_t complexes

Binding of DSG-crosslinked Rho*•G_t-LMNG complexes to sConA yielded triple sConA-Rho*•G_t complexes, which were isolated by size exclusion chromatography (Fig. 3A). The triple complex elution peak was dramatically shifted compared to the elution peak of Rho*•G_t complexes (Fig. 2A) indicating the formation of larger structures. TEM analysis of negatively stained sConA-Rho*•G_t complexes (Fig. 3B, upper panel) and calculation of 2D class averages from manually selected particles revealed elongated structures with lengths of 325±12 Å (Fig. 3B, bottom panel). These complexes were composed of two elongated densities lying parallel to each other in the middle of the complex and facing two bi-modal densities on each side (Fig. 3C). The bi-modal densities correspond to the Rho*•G_t-LMNG complex displayed in Fig. 2D, in which G_t (wider domain) binds Rho (narrower domain) on the C-terminal side. The N-terminal side of Rho, however, binds to sConA to form the elongated triple complex. The width of the Rho densities was smaller in triple complexes than in some class averages of Rho*•G_t-LMNG complexes (Fig. 2C, bottom panel; Table 1), indicating a flexible arrangement of the Rho*•G_t pentamer with respect to sConA consistent with the flexibility of the mannose chain. A semi empirical model of the sConA-Rho*•G_t complex built based on views obtained from 2D projections and using the crystal structure of a ConA dimer (pdb: 1DQ4) and the model of the Rho*•G_t complex (Jastrzebska et al., 2011b) supports our model of the triple complex composition (Fig. 3D).

Asymmetry of Rho monomers in the Rho*•G_t complex

Our TEM analysis revealed that photoactivation promotes binding of heterotrimeric G_t to a Rho dimer. As a result of light activation, Rho's 11-*cis*-retinylidene chromophore isomerizes to all-*trans*-retinylidene followed by Schiff base linkage hydrolysis and release of all-*trans*-retinal (Jastrzebska et al., 2011a) unless a Rho*•G_t complex is formed. As shown previously (Jastrzebska et al., 2011b), this complex exhibits a UV-visible maximum absorption peak at 380 nm and contains only all-*trans*-retinal bound, indicating that G_t stabilizes the activated conformation of Rho and inhibits all-*trans*-retinal release from the retinal-binding pocket. Taking into account an asymmetric nature of the Rho*•G_t complex (the C-terminus of $G_{t\alpha}$ binds only one Rho) it is unlikely that both Rho monomers in this complex are structurally and functionally equal. To validate this hypothesis, we quantified the retinoid content in the Rho*•G_t complex and in the complex incubated with 9-*cis*-retinal. Because chromophore regeneration was performed while the Rho*•G_t was still bound to the sConA resin, excess retinoid was washed out and did not affect this analysis. Before 9-*cis*-retinal treatment the Rho*•G_t complex contained only all-*trans*-retinal (Fig. 4, top black chromatogram and model of yellow-grey Rho dimer with bound G_t) but the complex regenerated with 9-*cis*-retinal contained both all-*trans*-retinal and 9-*cis*-retinal in ~ 1:1 stoichiometry (Fig. 4, upper middle dark grey chromatogram and model of yellow-pink Rho dimer with bound G_t). To achieve chromophore release from the Rho molecule stabilized by G_t, a wash with the strong nucleophile hydroxylamine (NH_2OH) was required to promote Schiff base hydrolysis. The resulting complex was depleted of all-*trans*-retinal but still contained 9-*cis*-retinal, because ground-state Rho and 9-*cis*-retinal regenerated opsin called isoRho are not affected by this NH_2OH exposure (Fig. 4, lower middle grey chromatogram and model of grey-pink Rho dimer with bound G_t). Surprisingly, incubation of such complexes with 11-*cis*-retinal produced complexes containing both all-*trans*-retinal and 9-*cis*-retinal in a 1:1 molar ratio, but virtually lacking 11-*cis*-retinal (Fig. 4, bottom light grey chromatogram and model of yellow-pink Rho dimer with bound G_t).

DISCUSSION

Recent work attests the existence of pentameric complexes comprised of a GPCR dimer and a heterotrimeric G protein (Baneres et al., 2003; El Moustaine et al., 2012; Han et al., 2009;

Jastrzebska et al., 2011b; Pellissier et al., 2011). GPCR dimers such as the serotonin receptor 5-HT2C (Herrick-Davis et al., 2006; Herrick-Davis et al., 2012), the β_1-adrenergic receptor (Kobayashi et al., 2009), and the b2AR (Angers et al., 2001; Angers et al., 2000) have also been identified in living cells. Atomic force microscopy revealed Rho to be packed in rows of dimers in the native murine disc membrane (Fotiadis et al., 2003; Fotiadis et al., 2004; Liang et al., 2003) and biochemical analyses confirmed the existence of native Rho dimers (Jastrzebska et al., 2006; Jastrzebska et al., 2004; Suda et al., 2004). Finally, *in vivo* studies of the luteinizing hormone receptor provided compelling functional evidence of intermolecular communication between ligand-binding deficient and G protein activation deficient mutants (Rivero-Muller et al., 2010). In contrast, some GPCR monomers were found to induce a physiological response *in vitro* (Whorton et al., 2007; Whorton et al., 2008), and the crystal structure of the T4 lysozyme (T4L)-b2AR•Gs•nanobody complex indicates a binding stoichiometry of one receptor and one G protein (Rasmussen et al., 2011).

For understanding the molecular signal transduction mechanisms of GPCRs knowledge of their minimal functional unit is indispensable. Here we present results from experiments designed to validate that Rho exists as a dimer in native disc membranes and to demonstrate that the native Rho*•G_t complex is a heteropentamer. In addition, we show that each Rho molecule of the heteropentamer has different structural and functional properties (Jastrzebska et al., 2013). We used the carbohydrate-binding protein Concanavalin A to assemble the Rho*•G_t complex 'on column', and as tag to decorate the heteropentamer.

Rho contains two sugar groups that modify the opsin structure through an asparagine linkage: mannose $(Man)_3$ attached to Asp^{15} and N-acetyl glucosamine $(GlcNAc)_3$ attached to Asp^2 (Fukuda et al., 1982; Salom et al., 2012). Though ConA itself forms tetramers, succinylated ConA exists in dimeric form and provides two sugar binding sites (Gunther et al., 1973). Moreover, sConA only binds mannose and not N-acetyl-glucosamine (Lis and Sharon, 1973). Therefore only one Rho can bind to one sugar-binding site in sConA, and a single sConA dimer will bind two Rho monomers in 5 mM DDM, as illustrated in Fig. 1B. The elongated central domain of the sConA-Rho complex has the size and shape of negatively stained sConA (Fig. 1C), whereas domains at its ends have a size (40 ± 2 Å) that corresponds to a Rho monomer (Jastrzebska et al., 2006).

In 1 mM DDM, however, Rho exists as dimer as previously documented by blue native gel experiments, and images of negatively stained samples (Suda et al., 2004). Fig. 1D reveals particles exhibiting a length of 65±4 Å, a width of 56±4 Å, and a central stained cleft, features compatible with the structure of two Rho molecules in a side-by-side arrangement (Palczewski et al., 2000). Rho dimers have the capability not only of binding two sConA dimers in solution but also of keeping them in a side-by-side configuration by binding at both ends (Fig. 1E). This configuration is only possible if the Rho monomers are parallel, and directly proves that native Rho exists in a dimeric form which can be purified at low DDM concentrations.

DDM solubilized Rho dimers bound to a sConA column and activated by light present a platform to bind G_t. As previously demonstrated, this complex retains full biological activity, can be eluted from the column, and exhibits dimensions, shape and mass of a Rho*•G_t heteropentamer (Jastrzebska et al., 2011b). Here we have exchanged DDM with LMNG and determined the 3D map of Rho*•G_t-LMNG to understand the difference of the heteropentameric Rho*•G_t-LMNG and the (T4L)-b2AR•Gs•nanobody-LMNG described in (Westfield et al., 2011). As illustrated in Fig. 2 negatively stained particles, their class averages, and the new 3D map are similar to those of Rho*•G_t-DDM published previously (Jastrzebska et al., 2011b). The major difference is the stain exclusion volume resulting from

the detergent (Fig. 2D, right): LMNG forms a larger belt than DDM (Table 1). This is compatible with a larger mass of the Rho*•G_t-LMNG than the Rho*•G_t-DDM complex (Jastrzebska et al., 2011b) estimated from gel filtration (Fig. 2A), and in agreement with the belts different detergents form to keep a plant aquaporin tetramer in solution (Vahedi-Faridi et al., 2012). However, the size of the LMNG micelle we observed is much smaller than what has been reported in (Westfield et al., 2011), a discrepancy that we cannot resolve.

To complete our structural analysis, a triple sConA-Rho*•G_t complex was formed by incubating Rho*•G_t complexes in 1 mM DDM with sConA and isolating the resulting triple complex by gel filtration (Fig. 3A). Images of negatively stained complexes confirmed the finding that Rho dimers arrange sConA as side-by-side dimers, and further demonstrate the native arrangement of the Rho dimer (Figs. 3B and C). A rough model was assembled of the triple sConA-Rho*•G_t complex to illustrate our interpretation of these findings (Fig. 3D).

Our protocol to isolate the native functional Rho*•G_t complex lends itself to probe the capacity of Rho to bind different retinoid chromophores. Excess or weakly bound chromophore can be washed away before elution of the complex and chromophore extraction for quantitative HPLC analysis. While a full account of these experiments is presented elsewhere (Jastrzebska et al., 2013), the binding of 9-*cis*- *and* 11-*cis*-retinal to the Rho*•G_t complex is described here. As Fig. 4 demonstrates, all-*trans*-retinal is not released from the binding pocket of Rho*, probably as result of the bound $G_{t\alpha}$ C-terminus, whereas the other Rho releases all-*trans*-retinal. Regeneration with 9-*cis*-retinal consequently leads to a complex that houses equal amounts of all-*trans*-retinal and 9-*cis*-retinal, the latter bound to the Rho monomer without bound $G_{t\alpha}$. Because subsequent treatment with NH_2OH removes all-*trans*-retinal but not 9-*cis*-retinal, regeneration with 11-*cis*-retinal affects only the Rho* monomer with the bound $G_{t\alpha}$. Unexpectedly, the regenerated heteropentamer again houses equal amounts of all-*trans*-retinal and 9-*cis*-retinal bound, suggesting that Rho* is stabilized by G_t in its active conformation even after chromophore depletion. The rigid constraints of this protein promote isomerization of 11-*cis*-retinal to its all-*trans*-retinal conformation because only the latter can be accommodated in the chromophore-binding pocket of Meta II-like Rho.

In conclusion, visualization of a sConA-Rho complex and a triple sConA-Rho*•G_t complex presents direct evidence that the native complex formed between activated Rho and G_t, i.e., the minimal functional unit, is a Rho dimer bound to a single G_t heterotrimer. Moreover, once coupled to G_t each Rho molecule of the dimer features different structural and functional properties (Fig. 4; (Jastrzebska, 2012)). Although the physiological significance of this arrangement is still elusive, GPCR dimerization appears to be the rule rather than the exception (Gonzalez-Maeso, 2011; Khelashvili et al., 2010; Nemoto et al., 2011; Pandit et al., 2010). Compelling evidence for the existence of b2AR dimers in living cells (Angers et al., 2001; Angers et al., 2000) suggests that the solved T4L-b2AR•Gs•nanobody complex, which consists of one receptor and one G protein (Rasmussen et al., 2011), could be promoted by specific crystallization conditions and bound nanobody.

MATERIALS AND METHODS

Chemicals

N-dodecyl-β-D-maltoside and lauryl-maltose-neopentyl-glycol were purchased from Affymetrix (Santa Clara, CA). Guanosine 5′-3-*O*-(thio)triphosphate (GTPγS) and 9-*cis*-retinal was from Sigma (St. Louis, MO). 11-*cis*-retinal was a generous gift from Dr. R. Crouch (Medical University of South Carolina, Charleston, USA).

Purification of Rho

Bovine ROS membranes were prepared from fresh retinas under dim red light as described in (Papermaster, 1982). ROS were solubilized in DDM and Rho was purified by the $ZnCl_2$-opsin precipitation method (Okada et al., 2004). $ZnCl_2$ was removed by dialysis against 10 mM BTP, pH 7.5, 100 mM NaCl and 0.2 mM DDM. Rho concentrations were determined with a Cary 50 UV-visible spectrophotometer (Varian, Palo Alto, CA) by absorption at 500 nm using the absorption coefficient $\varepsilon = 40{,}600\ M^{-1}cm^{-1}$ (Wald, 1957). The dialyzed preparation with ~ 10 mg/ml Rho also contained ~ 16 mM DDM as determined by measuring the contact angle of a sessile drop (Kaufmann et al., 2006). Therefore the ratio of DDM/Rho (w/w) was kept in a range 0.8–1.2 to preserve the oligomeric organization of Rho (Suda et al., 2004).

Purification of G_t

Bovine ROS membranes were prepared from fresh retinas and G_t was purified by extraction with hypotonic buffer from 200 dark-adapted bovine ROS membranes as described in (Goc et al., 2008). Briefly, ROS membranes were re-suspended in 30 ml of isotonic buffer (20 mM HEPES, pH 7.5, 5 mM $MgCl_2$, 1 mM DTT, and 100 mM NaCl) and soluble proteins were removed by gentle homogenization followed by centrifugation at 25,000*g* at 4°C for 15 min. G_t then was extracted from the pellet in 30 ml of hypotonic buffer (5 mM HEPES, pH 7.5, 0.1 mM EDTA, and 1 mM DTT). Membranes were pelleted by centrifugation at 25,000*g* at 4°C for 30 min and the supernatant was saved for further purification. This extraction procedure was repeated twice. Combined supernatants were centrifuged at 25,000*g* for 60 min to remove ROS membrane contaminants, and then HEPES, pH 7.5, was added to a final concentration of 10 mM and $MgCl_2$ to a final concentration of 2 mM, each from 1 M stock solutions. The resulting sample was applied at a flow rate of 15 ml/h to a 10 × 100 mm column containing 5 ml of pentyl-agarose resin pre-equilibrated with buffer containing 10 mM HEPES, pH 7.5, 2 mM $MgCl_2$ and 1 mM DTT and the column was washed with 10 column volumes of the equilibrating buffer. Bound proteins were subsequently eluted with a 50 ml linear gradient of 0 to 0.5 M NaCl in the equilibrating buffer at a flow rate of 15 ml/h, and 1 ml fractions were collected. Fractions containing G_t were pooled and concentrated with a 30,000 NMWL Centricon device (Millipore, Billerica, MA). G_t then was purified to homogeneity on a tandem Superdex 200 gel filtration column equilibrated with buffer containing 10 mM HEPES, pH 7.5, 100 mM NaCl, 2 mM $MgCl_2$, and 1 mM DTT at 4°C (flow rate 0.4 ml/min with collection of 0.5 ml fractions). Fractions containing G_t were combined and concentrated with a 30,000 NMWL Centricon device (Millipore, Bilerica, MA) to ~ 10 mg protein/ml as determined by the Bradford assay (Bradford, 1976).

Purification of the Rho*•G_t complex

The Rho*•G_t complex was purified by sConA affinity chromatography followed by gel filtration as described in (Jastrzebska et al., 2011b). Briefly, the sConA affinity resin was prepared by coupling sConA (Vector Laboratories, CA) to CNBr-activated agarose (Santa Cruz Biotechnology Inc., Santa Cruz, CA) at a density of 8 mg sConA/ml of resin. Purified Rho was diluted to ~ 0.2 mg/ml in equilibration buffer and loaded onto the sConA column pre-equilibrated with equilibrating buffer (20 mM BTP, pH 6.9, containing 120 mM NaCl, 1 mM $MnCl_2$, 1 mM $CaCl_2$, 1 mM $MgCl_2$, 1 mM DTT and 0.5 mM DDM) at 0.5 ml/min and room temperature. The resin was washed with 5 column volumes of the same ice cold buffer and then illuminated for 10 min with a 150 Watt fiber light (Dolan Jenner Industries Inc., Boxborough, MA) delivered through a 480–520 nm band pass filter. Purified native G_t, diluted to ~ 0.2 mg/ml with equilibrating buffer, was applied to the column immediately after light exposure at 0.5 ml/min and washed with 10 column volumes of the above buffer. The complex then was eluted with the same buffer containing 200 mM α-methyl-D-

mannoside at 0.2 ml/min. One mM DSG (disuccinimidyl glutarate) crosslinker (Thermo Scientific, Rockford, IL) was added immediately to the eluted fractions (0.5 ml) containing Rho*•G_t and the crosslinking reaction was allowed to proceed for 2 h on ice. The reaction was terminated by 1 M Tris, pH 8.0, added to a final concentration of 50 mM and incubated for 15 min. Fractions then were pooled and concentrated to 200 μl with a 30,000 NMWL Centricon device and used for size exclusion chromatography. Protein was loaded onto a gel filtation column (SRT™ SEC-300, SEPAX-Technologies, Inc., Newark, DE) equilibrated with 20 mM BTP, pH 6.9, containing 120 mM NaCl, 1 mM $MgCl_2$, 1 mM DTT and 0.5 mM DDM. Fractions containing crosslinked Rho*•G_t complex separate from free Rho and G_t were pooled, concentrated and processed on the same gel filtration column to increase sample homogeneity. The peak fraction was used for analysis by transmission electron microscopy (TEM). To prepare the Rho*•G_t-LMNG complex, fractions containing the Rho*•G_t complex separated by gel filtration were pooled, concentrated to 100 μl and incubated with 100 μl of 10 mM LMNG solubilized in 20 mM BTP, pH 6.9, containing 120 mM NaCl, 1 mM $MgCl_2$, and 1 mM DTT. After 1 h of incubation on ice, protein was processed on the same gel filtration column equilibrated with 20 mM BTP, pH 6.9, containing 120 mM NaCl, 1 mM $MgCl_2$, 1 mM DTT and 0.05 mM LMNG. Peak fractions containing Rho*•G_t-LMNG were then used for TEM analyses.

Purification of sConA-Rho complexes

Purified Rho (200 μg) diluted to 1 mg/ml with 20 mM BTP, pH 6.9, containing 120 mM NaCl, 1 mM $MnCl_2$, 1 mM $CaCl_2$, 1 mM $MgCl_2$ and either 1 mM or 5 mM DDM was mixed with an equimolar concentration of sConA and incubated at 4 °C for 1 h following gel filtration through a SRT™ SEC-300 column (SEPAX-Technologies, Inc., Newark, DE) equilibrated with one of the two above DDM-containing buffers. Peak fractions containing sConA-Rho complexes were analyzed by TEM.

Purification of the sConA-Rho*•G_t complex

The Rho*•G_t complex purified in LMNG was incubated at 4 °C overnight with excess sConA in buffer composed of 20 mM BTP, pH 6.9, containing 120 mM NaCl, 1mM $MnCl_2$, 1 mM $MgCl_2$, 1 mM DTT and 0.05 mM LMNG. The triple sConA-Rho*•G_t complex was separated by size exclusion chromatography on a SRT™ SEC-300 gel filtration column equilibrated with the same buffer as above and peak fractions were analyzed by TEM.

TEM of negatively stained sConA-Rho*•G_t, sConA-Rho, and Rho*•G_t, complexes and sConA

All purified complexes were diluted to ~20 μg/ml. sCon A was resuspended in 20 mM BTP, pH 6.9, containing 120 mM NaCl, 1 mM $MnCl_2$, 1 mM $CaCl_2$, 1 mM $MgCl_2$ and a specified detergent to reach a 5–20 μg/ml concentration. Protein complexes were adsorbed for 1 min to glow-discharged, 400 mesh, carbon-coated grids (Quantifoil Micro Tools GmbH, Germany). Grids were washed with 4 drops of distilled H_2O and negatively stained with 2% (w/v) uranyl acetate. Both single film and double film sandwich negative staining methods were used (Cheng et al., 2006). Electron micrographs of Rho dimers were recorded with a Hitachi H-7000 electron microscope operated at 100 kV. sConA-Rho sample images were taken with either a Philips CM10 microscope (Philips, Eindhoven, Netherlands) operated at 80 kV or a FEI TF20 microscope operated at 200 kV (FEI, Eindhoven, Netherlands). Rho*•G_t, sConA-Rho*•G_t and sConA samples were visualized only with a TF20 microscope operated at 200 kV. Electron micrographs of Rho*•G_t complexes were recorded at 0° and 45° tilts on a TF20 Gatan Ultrascan 4k CCD (Gatan Inc, Pleasanton, CA 94588, USA). Magnification was determined by measuring the meridional reflection of co-prepared tobacco mosaic virus (TMV; kindly supplied by Dr. Ruben Diaz-Avalos (Diaz-Avalos and Caspar, 1998)).

Single particle analyses and image processing of sConA-Rho, Rho*•G_t, sConA-Rho*•G_t, and sConA

Image processing was performed with the EMAN2 software package (Tang et al., 2007). Particles of sConA-Rho, sConA-Rho*•G_t, and sConA were selected manually by using the BOXER feature of EMAN2. Class averages were calculated for sConA-Rho in 1 mM DDM from 240 projections, sConA-Rho in 5 mM DDM from 836 projections, sConA from 885 projections and sConA-Rho*•G_t in LMNG from 667 projections. Particles of Rho*•G_t complexes purified in DDM or LMNG were selected manually by using the tilt pair boxing feature of EMAN2. For CTF correction, a Wiener filter approach was implemented in the SEMPER package (Saxton, 1996), and applied to all images before particle selection. For images of tilted samples, the defocus was determined for 64 512^2 pixel subregions to define the tilt angle and axis. Strips with a defocus range $\Delta f < 50$ nm were selected, CTF-corrected and merged in the CTF-corrected image. This procedure facilitated particle selection (Vahedi-Faridi et al., 2012) and was used throughout the project, although the resolution of the final 3D map (29 Å) indicated that CTF correction could have been omitted. Ninety six class averages were calculated from the Rho*•G_t complexes recorded with TF20 at a tilt of 0° and 45° (12950 projections for Rho*•G_t in LMNG and 8934 projections for Rho*•G_t in DDM). Initial models were calculated from the two class average sets by using the RCT method as well as the statistical method implemented in EMAN2 (e2initialmodel generator), and initial models were refined against the respective data sets.

Modeling procedure

A model of Rho*•G_t previously constructed (Jastrzebska et al., 2011b) was found to fit well to the 3D map of the DSG crosslinked Rho*•G_t -LMNG. As detailed in the supplementary information (Jastrzebska et al., 2011b), this model was built based on the intact G_t heterotrimer from the 1GOT structure, a Rho dimer featuring a two-fold dimer axis in between Helix IV and Helix V of adjacent rhodopsin protamers, and the 3DQB structure of opsin, which contains the C terminus of alpha from G_t bound, allowing G_t to be positioned. The triple sConA-Rho*•G_t complex was built from this model and a crystal structure of a ConA dimer (PDB 1DQ4). Two ConA dimers were arranged to mimic the features of the two elongated domains in the center of the triple complex. Rho*•G_t complexes were then placed at both ends of the sConA dimers in an arrangement dictated by the sugar moieties and respective binding sites.

Retinoid analyses

Rho*•G_t or chromophore-regenerated complexes (~100 μg protein) were denatured for 30 min at room temperature with 50% CH_3OH in the presence of 40 mM NH_2OH. The resulting retinal oximes were extracted with 300 μl of hexane and their isomeric content was determined after normal phase HPLC with an Ultrasphere-Si, 5 μm; 4.5 × 250 mm column (Beckman, San Ramon, CA). Retinoids, eluted isocratically with 10% ethyl acetate in hexane at a flow rate of 1.4 ml/min, were detected by their absorption at 360 nm or 325 nm (Garwin and Saari, 2000; Van Hooser et al., 2000) and quantified based on areas under corresponding chromatography peaks. Retinal oxime concentrations were calculated based on standard curves representing correlations between areas and peaks of synthetic standards for each retinal oxime isomer.

Supplementary Material

Refer to Web version on PubMed Central for supplementary material.

Acknowledgments

We thank Drs. Leslie T. Webster Jr., Phoebe L. Stewart, and members of the Palczewski laboratory for helpful comments on the manuscript, Dr. David Lodowski for his advice about building the model of the triple complex. This work was supported by National Institutes of Health grants EY008061 and EY019478, and the Swiss National Foundation grant 3100A0-108299 to AE who belongs to the Transcontinental EM Initiative for Membrane Protein Structure (TEMIMPS), which is a center for membrane protein structure determination funded by the NIH Protein Structure Initiative under grant U54GM094598. KP is John Hord Professor of Pharmacology.

Abbreviations used

b2AR	β_2-adrenergic receptor
Bis-Tris propane	1,3-bis[tris(hydroxymethyl)-methylamino]propane
CTF	contrast transfer function
DDM	n-dodecyl-β-D-maltoside
DTT	dithiothreitol
GDP	guanosine diphosphate
GTP	guanosine 5′-triphosphate
GTPγS	guanosine 5′-3-O-(thio)triphosphate
G_t	rod photoreceptor G protein (transducin)
GPCR	G protein-coupled receptor
HEPES	N-[2-hydroxyethyl]piperazine-N′-[2-ethanesulfonic acid]
HPLC	high performance liquid chromatography
LMNG	lauryl-maltose-neopentyl-glycol
Rho	rhodopsin
Rho*	photoactivated rhodopsin or Meta II
ROS	rod outer segment(s)
sConA	succinylated concanavalin A
T4L	T4 lysozyme
TMV	tobacco mosaic virus

References

Angers S, Salahpour A, Bouvier M. Biochemical and biophysical demonstration of GPCR oligomerization in mammalian cells. Life sciences. 2001; 68:2243–2250. [PubMed: 11358333]

Angers S, Salahpour A, Joly E, Hilairet S, Chelsky D, Dennis M, Bouvier M. Detection of beta 2-adrenergic receptor dimerization in living cells using bioluminescence resonance energy transfer (BRET). Proc Natl Acad Sci U S A. 2000; 97:3684–3689. [PubMed: 10725388]

Baneres JL, Martin A, Hullot P, Girard JP, Rossi JC, Parello J. Structure-based analysis of GPCR function: conformational adaptation of both agonist and receptor upon leukotriene B4 binding to recombinant BLT1. J Mol Biol. 2003; 329:801–814. [PubMed: 12787679]

Bradford MM. A rapid and sensitive method for the quantitation of microgram quantities of protein utilizing the principle of protein-dye binding. Anal Biochem. 1976; 72:248–254. [PubMed: 942051]

Cheng Y, Wolf E, Larvie M, Zak O, Aisen P, Grigorieff N, Harrison SC, Walz T. Single particle reconstructions of the transferrin-transferrin receptor complex obtained with different specimen preparation techniques. J Mol Biol. 2006; 355:1048–1065. [PubMed: 16343539]

Choe HW, Kim YJ, Park JH, Morizumi T, Pai EF, Krauss N, Hofmann KP, Scheerer P, Ernst OP. Crystal structure of metarhodopsin II. Nature. 2011; 471:651–655. [PubMed: 21389988]

Diaz-Avalos R, Caspar DL. Structure of the stacked disk aggregate of tobacco mosaic virus protein. Biophys J. 1998; 74:595–603. [PubMed: 9449360]

El Moustaine D, Granier S, Doumazane E, Scholler P, Rahmeh R, Bron P, Mouillac B, Baneres JL, Rondard P, Pin JP. Distinct roles of metabotropic glutamate receptor dimerization in agonist activation and G-protein coupling. Proc Natl Acad Sci U S A. 2012; 109:16342–16347. [PubMed: 22988116]

Fotiadis D, Liang Y, Filipek S, Saperstein DA, Engel A, Palczewski K. Atomic-force microscopy: Rhodopsin dimers in native disc membranes. Nature. 2003; 421:127–128. [PubMed: 12520290]

Fotiadis D, Liang Y, Filipek S, Saperstein DA, Engel A, Palczewski K. The G protein-coupled receptor rhodopsin in the native membrane. FEBS Lett. 2004; 564:281–288. [PubMed: 15111110]

Fukuda MN, Papermaster DS, Hargrave PA. Structural analysis of carbohydrate moiety of bovine rhodopsin. Methods Enzymol. 1982; 81:214–223. [PubMed: 7098866]

Garwin GG, Saari JC. High-performance liquid chromatography analysis of visual cycle retinoids. Methods Enzymol. 2000; 316:313–324. [PubMed: 10800683]

Goc A, Angel TE, Jastrzebska B, Wang B, Wintrode PL, Palczewski K. Different properties of the native and reconstituted heterotrimeric G protein transducin. Biochemistry. 2008; 47:12409–12419. [PubMed: 18975915]

Gonzalez-Maeso J. GPCR oligomers in pharmacology and signaling. Molecular brain. 2011; 4:20. [PubMed: 21619615]

Gunther GR, Wang JL, Yahara I, Cunningham BA, Edelman GM. Concanavalin A derivatives with altered biological activities. Proc Natl Acad Sci U S A. 1973; 70:1012–1016. [PubMed: 4515602]

Han Y, Moreira IS, Urizar E, Weinstein H, Javitch JA. Allosteric communication between protomers of dopamine class A GPCR dimers modulates activation. Nat Chem Biol. 2009; 5:688–695. [PubMed: 19648932]

Herrick-Davis K, Weaver BA, Grinde E, Mazurkiewicz JE. Serotonin 5-HT2C receptor homodimer biogenesis in the endoplasmic reticulum: real-time visualization with confocal fluorescence resonance energy transfer. J Biol Chem. 2006; 281:27109–27116. [PubMed: 16857671]

Herrick-Davis K, Grinde E, Lindsley T, Cowan A, Mazurkiewicz JE. Oligomer size of the serotonin 5-hydroxytryptamine 2C (5-HT2C) receptor revealed by fluorescence correlation spectroscopy with photon counting histogram analysis: evidence for homodimers without monomers or tetramers. J Biol Chem. 2012; 287:23604–23614. [PubMed: 22593582]

Hofmann KP, Scheerer P, Hildebrand PW, Choe HW, Park JH, Heck M, Ernst OP. A G protein-coupled receptor at work: the rhodopsin model. Trends Biochem Sci. 2009; 34:540–552. [PubMed: 19836958]

Jastrzebska B, Palczewski K, Golczak M. Role of bulk water in hydrolysis of the rhodopsin chromophore. J Biol Chem. 2011a; 286:18930–18937. [PubMed: 21460218]

Jastrzebska B, Orban T, Golczak M, Engel A, Palczewski K. Asymmetry of the rhodopsin dimer in complex with transducin. FASEB J. 2013

Jastrzebska B, Fotiadis D, Jang GF, Stenkamp RE, Engel A, Palczewski K. Functional and structural characterization of rhodopsin oligomers. J Biol Chem. 2006; 281:11917–11922. [PubMed: 16495215]

Jastrzebska B, Maeda T, Zhu L, Fotiadis D, Filipek S, Engel A, Stenkamp RE, Palczewski K. Functional characterization of rhodopsin monomers and dimers in detergents. J Biol Chem. 2004; 279:54663–54675. [PubMed: 15489507]

Jastrzebska B, Ringler P, Lodowski DT, Moiseenkova-Bell V, Golczak M, Muller SA, Palczewski K, Engel A. Rhodopsin-transducin heteropentamer: three-dimensional structure and biochemical characterization. J Struct Biol. 2011b; 176:387–394. [PubMed: 21925606]

Jastrzebska B, Orban T, Golczak M, Engel A, Palczewski K. Asymmetry of the rhodopsin dimer in complex with transducin. FASEB J. 2012 submitted.

Kaufmann TC, Engel A, Remigy HW. A novel method for detergent concentration determination. Biophys J. 2006; 90:310–317. [PubMed: 16214861]

Khelashvili G, Dorff K, Shan J, Camacho-Artacho M, Skrabanek L, Vroling B, Bouvier M, Devi LA, George SR, Javitch JA, Lohse MJ, Milligan G, Neubig RR, Palczewski K, Parmentier M, Pin JP, Vriend G, Campagne F, Filizola M. GPCR-OKB: the G Protein Coupled Receptor Oligomer Knowledge Base. Bioinformatics. 2010; 26:1804–1805. [PubMed: 20501551]

Kobayashi H, Ogawa K, Yao R, Lichtarge O, Bouvier M. Functional rescue of beta-adrenoceptor dimerization and trafficking by pharmacological chaperones. Traffic. 2009; 10:1019–1033. [PubMed: 19515093]

Liang Y, Fotiadis D, Filipek S, Saperstein DA, Palczewski K, Engel A. Organization of the G protein-coupled receptors rhodopsin and opsin in native membranes. Journal Of Biological Chemistry. 2003; 278:21655–21662. [PubMed: 12663652]

Lis H, Sharon N. The biochemistry of plant lectins (phytohemagglutinins). Annu Rev Biochem. 1973; 42:541–574. [PubMed: 4599386]

Nemoto W, Fukui K, Toh H. GRIPDB - G protein coupled Receptor Interaction Partners DataBase. Journal of receptor and signal transduction research. 2011; 31:199–205. [PubMed: 21410407]

Okada T, Sugihara M, Bondar AN, Elstner M, Entel P, Buss V. The retinal conformation and its environment in rhodopsin in light of a new 2.2 A crystal structure. J Mol Biol. 2004; 342:571–583. [PubMed: 15327956]

Orban T, Jastrzebska B, Gupta S, Wang B, Miyagi M, Chance MR, Palczewski K. Conformational dynamics of activation for the pentameric complex of dimeric G protein-coupled receptor and heterotrimeric G protein. Structure. 2012; 20:826–840. [PubMed: 22579250]

Palczewski K. G protein-coupled receptor rhodopsin. Annu Rev Biochem. 2006; 75:743–767. [PubMed: 16756510]

Palczewski K, Kumasaka T, Hori T, Behnke CA, Motoshima H, Fox BA, Le Trong I, Teller DC, Okada T, Stenkamp RE, Yamamoto M, Miyano M. Crystal structure of rhodopsin: A G protein-coupled receptor. Science. 2000; 289:739–745. [PubMed: 10926528]

Pandit SB, Brylinski M, Zhou H, Gao M, Arakaki AK, Skolnick J. PSiFR: an integrated resource for prediction of protein structure and function. Bioinformatics. 2010; 26:687–688. [PubMed: 20080513]

Papermaster DS. Preparation of retinal rod outer segments. Methods Enzymol. 1982; 81:48–52. [PubMed: 6212746]

Pellissier LP, Barthet G, Gaven F, Cassier E, Trinquet E, Pin JP, Marin P, Dumuis A, Bockaert J, Baneres JL, Claeysen S. G protein activation by serotonin type 4 receptor dimers: evidence that turning on two protomers is more efficient. J Biol Chem. 2011; 286:9985–9997. [PubMed: 21247891]

Rasmussen SG, DeVree BT, Zou Y, Kruse AC, Chung KY, Kobilka TS, Thian FS, Chae PS, Pardon E, Calinski D, Mathiesen JM, Shah ST, Lyons JA, Caffrey M, Gellman SH, Steyaert J, Skiniotis G, Weis WI, Sunahara RK, Kobilka BK. Crystal structure of the beta2 adrenergic receptor-Gs protein complex. Nature. 2011; 477:549–555. [PubMed: 21772288]

Rivero-Muller A, Chou YY, Ji I, Lajic S, Hanyaloglu AC, Jonas K, Rahman N, Ji TH, Huhtaniemi I. Rescue of defective G protein-coupled receptor function in vivo by intermolecular cooperation. Proc Natl Acad Sci U S A. 2010; 107:2319–2324. [PubMed: 20080658]

Sakmar TP, Menon ST, Marin EP, Awad ES. Rhodopsin: insights from recent structural studies. Annu Rev Biophys Biomol Struct. 2002; 31:443–484. [PubMed: 11988478]

Salom D, Wang B, Dong Z, Sun W, Padayatti P, Jordan S, Salon JA, Palczewski K. Post-translational modifications of the serotonin type 4 receptor heterologously expressed in mouse rod cells. Biochemistry. 2012; 51:214–224. [PubMed: 22145929]

Salom D, Lodowski DT, Stenkamp RE, Le Trong I, Golczak M, Jastrzebska B, Harris T, Ballesteros JA, Palczewski K. Crystal structure of a photoactivated deprotonated intermediate of rhodopsin. Proc Natl Acad Sci U S A. 2006; 103:16123–16128. [PubMed: 17060607]

Saxton WO. Semper: Distortion Compensation, Selective Averaging, 3-D Reconstruction, and Transfer Function Correction in a Highly Programmable System. J Struct Biol. 1996; 116:230–236. [PubMed: 8812977]

Scheerer P, Park JH, Hildebrand PW, Kim YJ, Krauss N, Choe HW, Hofmann KP, Ernst OP. Crystal structure of opsin in its G-protein-interacting conformation. Nature. 2008; 455:497–502. [PubMed: 18818650]

Standfuss J, Edwards PC, D'Antona A, Fransen M, Xie G, Oprian DD, Schertler GF. The structural basis of agonist-induced activation in constitutively active rhodopsin. Nature. 2011; 471:656–660. [PubMed: 21389983]

Suda K, Filipek S, Palczewski K, Engel A, Fotiadis D. The supramolecular structure of the GPCR rhodopsin in solution and native disc membranes. Mol Membr Biol. 2004; 21:435–446. [PubMed: 15764373]

Tang G, Peng L, Baldwin PR, Mann DS, Jiang W, Rees I, Ludtke SJ. EMAN2: an extensible image processing suite for electron microscopy. J Struct Biol. 2007; 157:38–46. [PubMed: 16859925]

Vahedi-Faridi A, Jastrzebska B, Palczewski K, Engel A. 3D imaging and quantitative analysis of small solubilized membrane proteins and their complexes by transmission electron microscopy. Journal of electron microscopy. 2012

Van Eps N, Preininger AM, Alexander N, Kaya AI, Meier S, Meiler J, Hamm HE, Hubbell WL. Interaction of a G protein with an activated receptor opens the interdomain interface in the alpha subunit. Proc Natl Acad Sci U S A. 2011; 108:9420–9424. [PubMed: 21606326]

Van Hooser JP, Garwin GG, Saari JC. Analysis of visual cycle in normal and transgenic mice. Methods Enzymol. 2000; 316:565–575. [PubMed: 10800702]

Wald G. The chemistry of visual excitation. Bibliotheca ophthalmologica : supplementa ad ophthalmologica. 1957; 12:173–188. [PubMed: 13382750]

Westfield GH, Rasmussen SG, Su M, Dutta S, DeVree BT, Chung KY, Calinski D, Velez-Ruiz G, Oleskie AN, Pardon E, Chae PS, Liu T, Li S, Woods VL Jr, Steyaert J, Kobilka BK, Sunahara RK, Skiniotis G. Structural flexibility of the G alpha s alpha-helical domain in the beta2-adrenoceptor Gs complex. Proc Natl Acad Sci U S A. 2011; 108:16086–16091. [PubMed: 21914848]

Whorton MR, Bokoch MP, Rasmussen SG, Huang B, Zare RN, Kobilka B, Sunahara RK. A monomeric G protein-coupled receptor isolated in a high-density lipoprotein particle efficiently activates its G protein. Proc Natl Acad Sci U S A. 2007; 104:7682–7687. [PubMed: 17452637]

Whorton MR, Jastrzebska B, Park PS, Fotiadis D, Engel A, Palczewski K, Sunahara RK. Efficient coupling of transducin to monomeric rhodopsin in a –phospholipid bilayer. J Biol Chem. 2008; 283:4387–4394. [PubMed: 18033822]

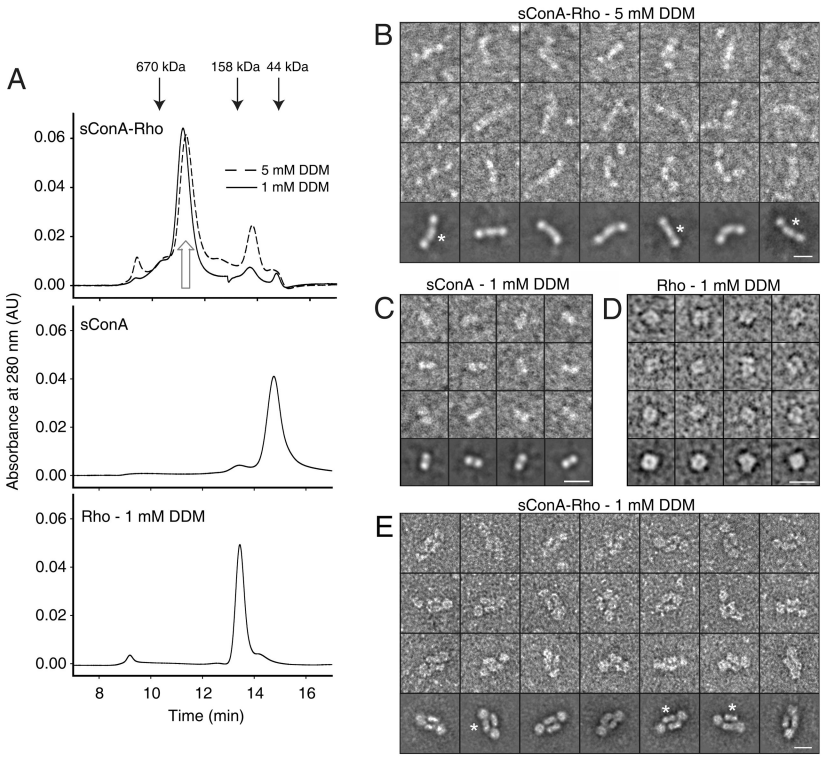

Figure 1. Purification and visualization of sConA-Rho complexes

A) Gel filtration elution profile of the sConA-Rho complex in 1 mM DDM (solid line, top panel) and 5 mM DDM (broken line, top panel) compared with sConA (middle panel) and Rho alone (bottom panel). Open arrow indicates the peak fraction used for further characterization. Black arrows on top of the chromatogram indicate the elution profiles of molecular standards: thyroglobulin (670 kDa), IgG (158 kDa) and ovalbumin (44 kDa). Negatively stained and manually selected particles (3 top rows) and class averages (bottom row) obtained from selected particles of sConA-Rho complex purified in 5 mM DDM (B), sConA alone (C), Rho dimer purified in 1 mM DDM (D), and sConA-Rho complex purified in 1 mM DDM (E). sConA exhibits a bi-modal density (C) that is seen in class averages of both types of sConA-Rho complexes (*). Scale bars 100 Å.

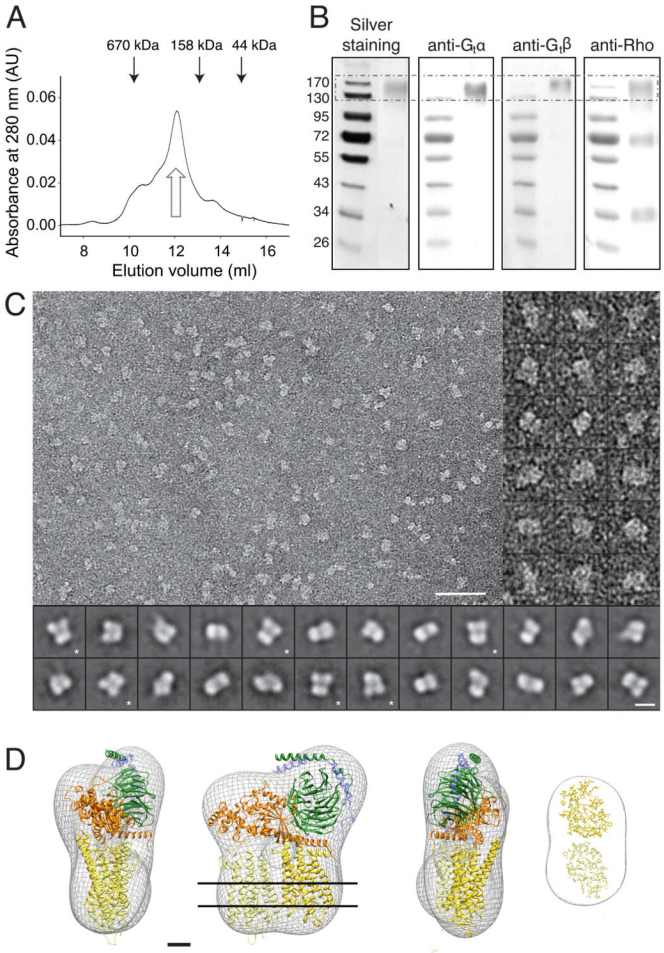

Figure 2. Visualization and 3D reconstruction of the Rho*•G_t-LMNG complex

A) Gel filtration elution profiles of purified DSG-crosslinked Rho*•G_t complexes in LMNG. Open arrow indicates protein elution fraction used for further analyses. Black arrows on top of the chromatogram indicate the elution profiles of molecular standards: thyroglobulin (670 kDa), IgG (158 kDa) and ovalbumin (44 kDa). B) Silver-stained SDS-PAGE gel and immunoblot analyses of the peak fraction in A incubated with antibodies against $G_{t\alpha}$, $G_{t\beta}$ and Rho. Identification of DSG-crosslinked Rho*•G_t complexes is indicated by the broken line frame. C) TEM image of negatively stained Rho*•G_t-LMNG complexes (upper left panel). Scale bar 500 Å. Negatively stained and manually selected particles of Rho*•G_t-LMNG (upper right panel). 2D class averages obtained from particles selected from images taken at 0° tilt (bottom panel). Scale bar 100 Å. Asterisks indicate projections of class averages clearly displaying a tri-lobed morphology of the complex. D) Semi-empirical model of the Rho*•G_t complex fitted into 3D maps calculated from projections of DSG-crosslinked Rho*•G_t complex purified in LMNG. Based on the Fourier shell correlation function, the resolution of the map obtained for the Rho*•G_t-LMNG was determined to 29 Å. The 20 Å thick slice on the right shows the volume occupied by the detergent. Scale bar 20 Å. In the Rho*•G_t complex, the activated Rho monomer in the dimer is depicted in dark yellow and the second Rho is shown in light yellow. $G_{t\alpha}$, $G_{t\beta}$, $G_{t\gamma}$ are colored orange, green and pale blue, respectively.

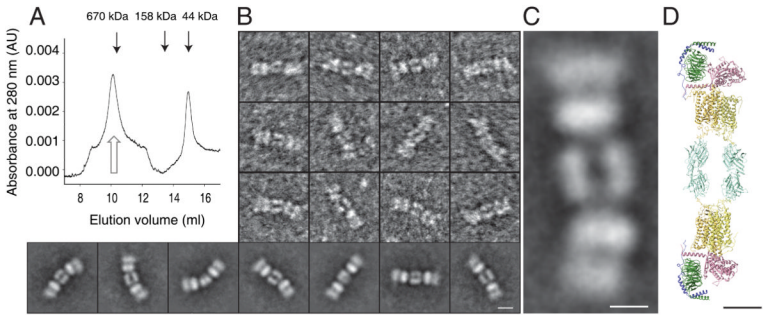

Figure 3. Purification and visualization of the triple sConA-Rho*•G_t complex

A) Gel filtration elution profile of sConA-Rho*•G_t-LMNG complex. Open arrow indicates peak fraction used for further characterization. B) Negatively stained and manually selected particles (3 top rows) and class averages (bottom row) obtained from selected particles of sConA-Rho*•G_t complex. C) Magnified 2D projection of the sConA-Rho*•G_t complex. D) Semi-empirical model of the sConA-Rho*•G_t complex composed of two Rho*•G_t complexes and two sConA dimers. This model was built based on views obtained from 2D projections and using a known crystal structure of a sConA dimer (pdb: 1DQ4) and a model of the Rho*•G_t complex (Jastrzebska et al., 2011b). Scale bars 50 Å. In the Rho*•G_t complex, activated Rho in the dimer is depicted in dark yellow and the second Rho is shown in light yellow. $G_{t\alpha}$, $G_{t\beta}$, $G_{t\gamma}$ are colored dark salmon, light green and pale blue, respectively. sConA dimers are shown in cyan.

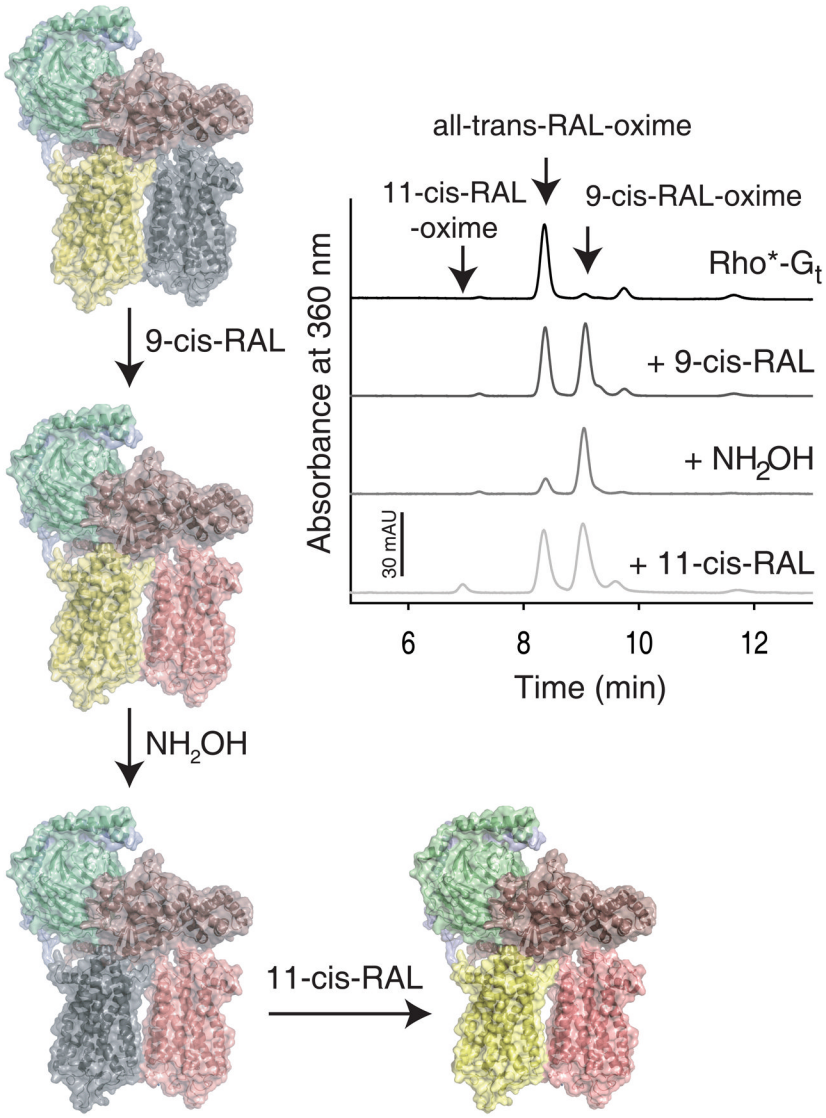

Figure 4. Asymmetry of Rho monomers in Rho*•G_t complex

The Rho*•G_t complex prepared on a sConA affinity resin (shown as a yellow-grey dimer bound to G_t) was first regenerated with 9-*cis*-retinal (shown as a yellow-pink dimer bound to G_t) followed by treatment with NH_2OH (modeled as a grey-pink dimer bound to G_t) and then regenerated with 11-*cis*-retinal (shown as a yellow-pink dimer bound to G_t). Isocratic analyses of retinoid oximes extracted from Rho*•G_t (black line), either regenerated with 9-*cis*-retinal (dark grey line), treated with NH_2OH (grey line) or regenerated with 11-*cis*-retinal (light grey line) are shown. Though only all-*trans*-retinal was detected in the Rho*•G_t complex, a mixture of all-*trans*-retinal and 9-*cis*-retinal with about a 1:1 stoichiometry was found in the Rho*•G_t complex incubated with 9-*cis*-retinal. Treatment of this regenerated complex with NH_2OH caused a significant reduction in all-*trans*-retinal. However, incubation of this complex with 11-*cis*-retinal resulted in formation a complex carrying a mixture of all-*trans*-retinal and 9-*cis*-retinal in about a 1:1 molar ratio.

TABLE 1

Statistical analyses of particle sizes.

Preparation	Length of the complex (Å)	n of particles	Width of Rho(Å)	Detergent belt thickness (Å)[e]
sConA-Rho_5 mM DDM [a, c]	191 ± 13	14	40 ± 2	-
sConA-Rho_1 mM DDM [b, c]	195 ± 10	12	63 ± 4	-
sConA [a, c]	84 ± 3	14	-	-
Rho*•G_t_LMNG [a, d]	129 ± 7	15	107 ± 6	14 (15±5)
Rho*•G_t_DDM [a, d]	130 ± 7	15	91 ± 4	6 (11±4)
sConA-Rho*•G_t_LMNG [a, c]	325 ± 12	14	93 ± 5	-

Images were collected with a [a]Tf20 and a [b]CM10 transmission microscope. [c]Particles or [d]particle pairs from images collected at 0° and 45° tilt were selected manually by using the boxer or the pair-picking features of EMAN2. [e]The detergent belt thickness, T_{belt}, was calculated from the width of Rho, W_{Rho}, measured on a micrograph as $T_{belt}=(W_{Rho}-80)/2$, where the width of the protein is 80 Å. T_{belt} also was estimated from the difference of the iso-contoured 3D map and the fitted model measured on 3 sections (in brackets). The discrepancy between the width of Rho dimers in sConA-Rho-DDM and Rho*•G_t-DDM is due to the preferential orientation of the latter after adsorption to a carbon film.